Colloidal and chemical stabilities of iron oxide nanoparticles in aqueous solutions: the interplay of structural, chemical and environmental drivers

Edwige Demangeat, Mathieu Pédrot, Aline Dia, Martine Bouhnik-Le Coz, Fabien Grasset, Khalil Hanna, M. Kamagaté, Francisco Cabello-Hurtado

Environmental Science Nano

Accepted Manuscript

This article can be cited before page numbers have been issued, to do this please use: E. Demangeat, M. Pedrot, A. Dia, M. Bouhnik-Le-Coz, F. Grasset, K. Hanna, M. Kamagate and F. Cabello-Hurtado, *Environ. Sci.: Nano*, 2018, DOI: 10.1039/C7EN01159H.

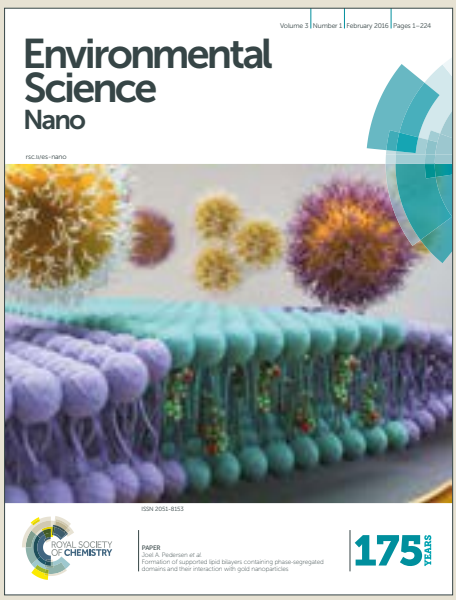

ROYAL SOCIETY OF CHEMISTRY

rsc.li/es-nano

View Article Online
DOI: 10.1039/C7EN01159H

Environmental significance statement

Amongst engineered nanoparticles, iron oxide nanoparticles (IONPs) appear particularly relevant toward the environment. Indeed, considering their potential uses in environmental fields (water and soil depollution, agrochemistry, etc.), it becomes critical to determine their behavior and fate in the environment. Their stability and reactivity are dependent upon the environmental parameters, and both intrinsic and surficial properties of IONPs. This work focused on the aggregation behavior of IONPs (especially magnetite, maghemite, hematite), their chemical transformation (oxidation of magnetite) and the impact of a surface coating that mimic natural interactions possibly occurring in the environment. Understanding these interactions and transformations will thus bring key insights regarding the mobility, bioavailability and chemical reactivity of IONPs in prevailing environmental conditions.

View Article Online
DOI: 10.1039/C7EN01159H

Environmental Science: Nano

ARTICLE

Colloidal and chemical stabilities of iron oxide nanoparticles in aqueous solutions: the interplay of structural, chemical and environmental drivers

Received 29th November 2017,
Accepted 00th January 20xx

DOI: 10.1039/x0xx00000x

www.rsc.org/

E. Demangeat,[a] M. Pédrot,[a] A. Dia,[a] M. Bouhnik-le-Coz,[a] F. Grasset,[b] K. Hanna,[c] M. Kamagate[c] and F. Cabello-Hurtado[d]

Nanoparticle (NP) stability in aqueous environments is dependent upon many parameters including environmental conditions, NP concentrations as well as NP intrinsic characteristics. In this study, the effects of pH and surface modifications on the colloidal and chemical stabilities of nanosized magnetite (Fe_3O_4), maghemite (γ-Fe_2O_3) and hematite (α-Fe_2O_3) are investigated. Because changes in surface charge affect the size distribution of NP, pH plays a key role in driving the colloidal stability. More NP aggregation is observed at pH values close to the pH of zero point of charge (pHzpc). Coating of magnetite with humic acid (HA) and phosphatidylcholine (PC) affects the electrostatic interactions and then the colloidal behavior of NP. The rapid transformation of magnetite into maghemite through air oxidation results in significant modification of both surface charge and specific surface area of NP. Because the maghemite almost exclusively formed µm-scale aggregates, the colloidal stability of magnetite is expected to be hindered in oxic environments. For hematite, the particle size distribution data emphasize the influence of both pH and intrinsic surface properties in colloidal stability. These findings may have strong implications for an accurate prediction of the transformation and mobility of Fe-nanoparticles under environmentally relevant conditions and thus their fate in nature.

Introduction

Understanding the prevailing processes controlling chemical exchanges at soil/water interfaces is an environmental priority with regards to their impacts on both ecosystems and soil services, as well as water resources. Iron (Fe) oxides are ubiquitous minerals constituent of soils, sediments, aquifers and geological materials[1, 2]. Their origin is also anthropogenic as they are increasingly used in various fields such as for industrial, medical and environmental purposes[3-6]. Iron oxides nanoparticles (NP) respective stability, specific surface area, porosity, dissolution rate as well as transformation kinetics are controlled by their mineral structure and determine their fate and behaviour in the environment[7]. Amongst them, iron oxide nanoparticles, which also occur as ubiquitous phases in both soils and waters, play a critical role in the chemical dynamics resulting from environmental condition changes since nano minerals are highly reactive[8, 9]. In the natural conditions, only a small fraction of engineered iron oxide NP persists in its original form[10]. Biotransformation, oxidation/reduction, dissolution, precipitation, sorption and photochemical transformation may occur amongst other biogeochemical driven processes[11, 12]. In turn, this transformation can affect the aggregation, mobility, biointeractions, uptake and fate of iron oxide NP in the environment as well as their impacts on the living environment[13].

Engineered iron oxide NP will become new tools for the treatment of contaminated waters and soils[14, 15]. As compared to conventional macroscale materials, nanomaterials exhibit a high surface-to-volume ratio and high reactivity. Thus, their colloidal size may give them high mobility in porous media and their properties allow them to be particularly suitable for the treatment of contaminated soils or aquifers. Iron oxide NP are involved in (i) the dechlorination of organic solvents (CCl_4, C_2Cl_4), (ii) the detoxification of pesticides (such as Lindane, DDT), (iii) the transformation of fertilizers (NO_3^-), and (iv) the immobilization of metals and metalloids (As, Pb, Cr, etc.)[16-18]. If remediation projects using iron oxide NP are currently focused on local-scale pollution, a scale change is initiated to act against diffuse pollution. Moreover, their use in nano-agrochemistry could be developed in the years ahead and would represent an intentional diffuse source of iron oxide NP within the environment[19]. A widespread use of iron oxide NP for *in situ* remediation or in agriculture also raises the question of their environmental compatibility.

Amongst engineered iron oxide NP of environmental concern, magnetite (Fe_3O_4), maghemite (γ-Fe_2O_3) and hematite (α-Fe_2O_3) are popular engineered iron oxide NP because of their biocompatibility and safety towards living organisms under certain conditions[20-22]. In particular, magnetite has shown an outstanding applicability in many research areas (e.g., semiconductor, magnetic resonance imaging, pigment, biomedicine, drug delivery, heterogeneous

[a] Univ. Rennes, CNRS, Géosciences Rennes - UMR 6118 – F- 35000 Rennes, France
[b] Univ. Rennes, CNRS-Saint-Gobain-NIMS-UMI LINK 362-J-305-044, Tuskuba, Japan
[c] Univ. Rennes, ENSCR- CNRS, ISCR (Institut des Sciences Chimiques de Rennes) - UMR 6226 F-35000 Rennes, France
[d] Univ. Rennes, CNRS, Ecobio - UMR 6553 - F-35000 Rennes, France

View Article Online
DOI: 10.1039/C7EN01159H
ARTICLE Journal Name

catalysis, and environmental remediation)[23, 24, 25] due to its unique magnetic properties and easy manipulation for control of morphologies, particle size, and Fe^{II}/Fe^{III} stoichiometry[26, 27]. However, determination of magnetite compositions which is highly sensitive to the preparation conditions is not a trivial task, particularly for nanoscale particles with a higher surface-to-volume ratio. Magnetite compositions range, without modification of the crystal structure, from that of stoichiometric Fe_3O_4, with 8 Fe^{3+} ions in tetrahedral and 8 Fe^{2+} + 8 Fe^{3+} ions in octahedral sites, to that of maghemite γ-$Fe^{III}_2O_3$ (considered as an extreme example of a non-stoichiometric magnetite) with only Fe^{3+} ions in both tetrahedral and octahedral sites. As compared to these iron oxides, hematite has only one type of cation, Fe^{3+} in its structure[28, 29].

In aqueous solution, iron oxides (IO) are amphoteric solids that acquire a surface charge in the protonation and deprotonation reactions of Fe-OH surface sites. The ensuing electrostatic, steric or combined stabilization layers that develop at the surface of the particles are significant in driving iron oxide NP colloidal stability[30]. The interfacial equilibrium at the surface of iron oxide NP is thus affected by the adsorption and desorption of the various constituents of the soil and soil solution in addition to the solution pH[31, 32]. The surface charge of iron oxide NP is also dependent upon their own structural organization such as isomorphic substitutions, which give iron oxide NP permanent charges.

As part of the Natural Organic Matter (NOM) occurring within soils and waters, macromolecular polyfunctional humic acid (HA), which displays a particular affinity for metal ions and their various acidic functional groups (carboxylic, phenolic, carbonyl), favours the formation of surface complexes on the Fe-OH sites of iron oxides via chemisorption[33]. As a consequence, interactions between iron oxide NP and HA should be further investigated. Several studies have shown that, in aqueous solution, the HA coating on iron oxide NP likely imparts a negative charge to the nanoparticle surfaces, increasing their surface potential and the ensuing propensity to stabilize iron oxide NP against aggregation[34-36]. Nevertheless, Hadju et al.[37] demonstrated that coating magnetite with HA could either foster or hinder Fe_3O_4-NP colloidal stability depending on the amount of HA present at the mineral surfaces. Other natural constituents such as amphiphilic phospholipids (integral major component of cell membranes) likely affect iron oxide NP stability. Using phospholipids as a coating on pyrite surfaces, Hao et al.[38] demonstrated that surface-bound lipids inhibit the iron core from oxidizing, even in the presence of bacteria, by forming a hydrophobic pocket[38, 39]. In addition, several authors have shown that a phospholipid coating likely decreases nanoparticle size dispersion and favours narrow-sized nanoparticles[40, 41]. Furthermore, the instability of magnetite in air causes NP to undergo a partial oxidation to maghemite (γ-Fe_2O_3), ending up with a core-shell structure in which the thickness of the oxidized layer is a function of the particle size[42, 43]. This phase transformation directly affects the surficial properties and internal characteristics of NP, which are deeply involved in driving iron oxide chemical stability and reactivity[44, 45].

In the environment, soils and soil solutions are prior interfaces for iron oxide NP interactions[46] occurring at mineral surfaces and in water. In addition to particle interactions, NP are prone to various chemical and physical modifications which foster the complexity of the reactions and likely affect both NP stability and reactivity. Electrostatic, steric or combined electrosteric forces can result from these interactions and promote repulsive forces whereas Van der Waals and magnetic dipolar interactions foster attraction between particles that likely aggregate. The intrinsic physicochemical properties of iron oxide NP (size, shape, surface area, chemistry, superparamagnetism, etc.), their ensuing high reactivity, together with the surrounding solution composition (dissolved species, pH, ionic strength, nanoparticle concentration), are the main drivers of iron oxide NP chemical and colloidal stability in aqueous media[47, 48].

Considering the geochemical, biological and technological significance of iron oxide NP[49], understanding the mechanisms of their stability may turn out to be relevant to unravel the fate and behaviour of iron oxide NP in the environment as well as their impacts on living organisms. Therefore, the aim of this work is to investigate the dual colloidal and chemical stability of magnetite NP in order to (i) understand the effects of their intrinsic properties (size, morphology, surface chemistry) and those of the environmental drivers (especially the effect of pH) on their aggregation state, (ii) assess the oxidation kinetics of magnetite, (iii) investigate the link between colloidal and chemical stability of NP, as well as (iv) identify the resulting environmental impacts. Hematite has also been studied to better understand the impact of intrinsic structural properties on iron oxide NP colloidal stability as the structure of hematite differs from both magnetite and maghemite**.** Indeed hematite NP size and morphology as well as internal crystal structure, generally confer a higher stability and crystallinity to hematite. Last, the method we chose to study the iron oxide NP aggregation state allowed us to study their size distribution over a wide range of sizes (that spread from one tenth of a nm to µm-scale aggregates) which allowed us to determine NP behavior in a context comparable to those observed in natural waters.

Experimental

Iron oxide nanoparticles and coated magnetite NP

Synthesis of bare iron oxide NP. Magnetite (Fe_3O_4) was prepared by the co-precipitation of iron salts according to the modified literature procedure [50, 51]. In brief, $FeCl_2.4H_2O$ (1.988 g) and $FeCl_3.6H_2O$ (5.406 g) were dissolved in 5 mL HCl (2 M) and 20 mL H_2O, respectively, and then mixed with magnetic stirring to obtain an iron solution with a molar ratio of Fe(II)/Fe(III) = 0.5. Magnetite NP were then precipitated by the dropwise addition of the iron salt solution into a 0.7 M NaOH-$NaNO_3$ base solution (250 mL). The black precipitate was left to settle in anaerobic conditions for a few hours to get rid of the supernatant. Three washings were then conducted in anaerobic conditions with deoxygenated deionized water and 5 10^{-3} M NaCl solution.

View Article Online
DOI: 10.1039/C7EN01159H

Maghemite (ɣ-Fe_2O_3) was synthesized following the method of Anna et al.[52], through the oxidation of the previously synthesized magnetite by adding 5 wt% NaOCl aqueous solution (16 mL) and sonicating for 2 hours. The solid product was magnetically separated and washed with water.

Hematite (α-Fe_2O_3) was synthesized by the forced hydrolysis of acid Fe(III) salt solutions at 98°C from 0.02 M $Fe(NO_3)_3$ following the protocol described in Schwertmann & Cornell (2003)[1].

Coatings with humic acid and phosphatidylcholines. Fe_3O_4-NP were coated with HA (Elliott Soil Humic Acid Standard IV) and PC (1, 2-bis (10, 12-tricosadiynoyl)-sn-glycero-3-phosphocholine - CAS Registry Number: 76078-28-9) to model a natural surface modification. The coating was carried out by physical interactions between the dissolved organic species (HA and PC) and a concentrated fraction of the Fe_3O_4-solution. Humic acid (0.2 g) was dissolved in 10 mL NaOH (1 M) and the obtained HA-solution was completed to 56 mL with deionized water. A similar PC-solution was obtained by dissolution in deionized water and ultrasonication. Fourty-four mL of a 6.0 g L^{-1} Fe_3O_4-NP solution was then added to each organic stock solution and each 100 mL of solution was shaken for 48 hours. At the end of the interaction, five washings were performed to remove the uncoated materials present in the supernatant after centrifugation.

Nanoparticle mass concentration measurement. The concentration of the iron oxide NP solution was inferred from the ICP-MS measurements of iron on triplicate samples for the iron oxide NP solutions and then recalculated regarding the total theoretical iron content of the minerals. Each NP sample was digested with sub-boiled nitric acid (14.6 M HNO_3) at 85°C, and then re-solubilized in 0.37 M HNO_3 after complete evaporation before measurement. Major- and trace-element concentrations were determined by ICP-MS (Agilent 7700x), using rhenium and rhodium as the internal standard. The international geostandard SLRS-5 was used to check the validity and reproducibility of the results[53].

Characterization

Size, morphology and surface properties. The morphology and individual particle size of Fe_3O_4, HA-Fe_3O_4, PC-Fe_3O_4, ɣ-Fe_2O_3 and α-Fe_2O_3 were determined using High Resolution Transmission Electron Microscopy (HR-TEM) with a JEOL2100F (voltage 200 kV). Specimens were prepared by drop-casting diluted Fe-NP suspensions on 300 mesh Au-grids supported with carbon film.

The specific surface area of the iron oxides was determined by multipoint N_2–BET (Brunauer Emmett Teller) analysis using a Coulter (SA 3100) surface area analyzer.

The pH of zero point of charge was determined by potentiometric titrations, which were conducted with 1 and 2 g L^{-1} of solid at three ionic strengths (10^{-2}, 5.10^{-2}, and 10^{-1} M of NaCl). The suspension was purged with nitrogen gas to remove CO_2 in a double-walled Pyrex cell, which was kept at constant temperature by circulating water from thermostat. Titrations were conducted from 4 to 10 by addition of titrant solutions (HCl or NaOH).

Synthesized NP were characterized using X-ray powder diffraction (XRD). XRD data were collected with a Johanson monochromator using CuK_α radiation (λ = 1.5406 A). The X-ray diffractograms were found to be identical with the expected oxides.

Laser particle size analyses allowed the characterization of the size distribution of magnetite, maghemite, hematite and HA- and PC-

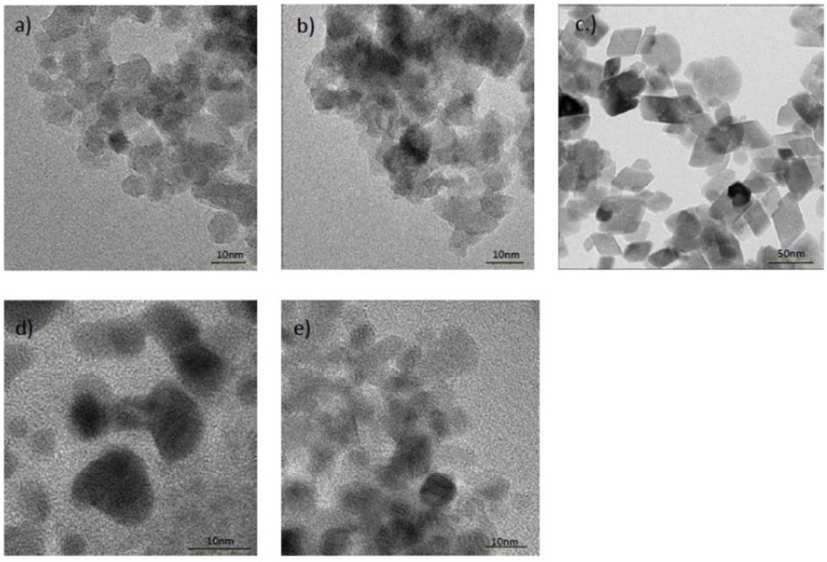

Fig. 1: High Resolution TEM (HRTEM) images of a) Fe_3O_4, b) ɣ-Fe_2O_3, c) α-Fe2O3, d) HA-Fe_3O_4 and e) PC-Fe_3O_4

View Article Online
DOI: 10.1039/C7EN01159H
ARTICLE Journal Name

NP	TEM (nm)	BET ($m^2 g^{-1}$)	pHzpc
Magnetite	7 ± 2	115	5.8
Maghemite	6 ± 2	131	7 - 8.4
Hematite	28 ± 5 39 ± 5	49	8.2

Table 1: Physicochemical properties of a) Fe_3O_4, b) γ-Fe_2O_3 and c) α-Fe_2O_3 obtained from TEM, BET analyses and potentiometric titration.

coated magnetite to study the colloidal stability and, conversely, their aggregation behaviour. Assuming measurements on spherical particles, the technique provided sizes amongst the 100 size classes detected, which spread from 0.04 µm to 2500 µm. Analyses were performed by the laser diffraction technique on a Cilas1180 analyzer. Measurements were taken on each bare iron oxide (Fe_3O_4, γ-Fe_2O_3 and α-Fe_2O_3) and coated magnetite (HA-Fe_3O_4 and PC-Fe_3O_4) at five different pH values (pH = 3, 4, 5, 6, 7.5). Particle size measurements were performed by adjusting obscuration values allowing for an optimal analysis. Then, the pH was equilibrated with HCl and NaOH solutions (0.1 M and 0.1 M to 1.0 M, respectively) until the target pH was reached.

ATR-FTIR. Attenuated total reflectance-Fourier transform infrared (ATR-FTIR) spectra were recorded in the 780 - 1800 cm^{-1} region on an IS50 Nicolet spectrometer equipped with a KBr beam splitter and a liquid Nitrogen cooled MCT (Mercury Cadmium Telluride) detector. A nine-reflection diamond ATR accessory (Durasampl*IR* ™, SensIR Technologies) was used for acquiring spectra of wet samples. The resolution of the single beam spectra was 4 cm^{-1}. Prior to ATR-FTIR analyzes, tubes containing coated NP were centrifuged at 4110 RCF for 30 min. Wet mineral pastes were directly and uniformly applied to the diamond ATR crystal then covered with a lid of a flow-through cell to prevent the evaporation of water. ATR-FTIR spectra were then recorded immediately.

To monitor potential dissolution of NP, aliquots were collected at each pH value, centrifuged and the supernatants were filtered using 5 KDa ultrafiltration cells (from Sartorius) in order to stop NP on the filter. ICP-MS was then performed to measure total iron concentration.

Oxidation kinetics. A NP suspension (2.5 g L^{-1}), prepared in anoxic conditions, was placed outside the glove box under air ambient environment to monitor the oxidation. The total Fe(II)/Fe(III) ratio in suspension was then analyzed versus time over nine days. For each sampling, two aliquots were placed in an anaerobic chamber: the first aliquot contained bulk solution and the second was filtered (0.2 µm, Whatman). NP suspension was dissolved during 12h using 0.6 N HCl while filtered NP were directly dissolved. Dissolved Fe(II) and Fe(III) concentrations were then determined using the phenanthroline method[54, 55] and the bulk Fe(II) content turned out to be very close to that determined by acid digestion on the filtered solid. The amount of magnetite bound-Fe(II) ([Fe(II)] bound = [Fe(II)]tot – [Fe(II)]aq) was used to calculate the effective Fe(II)/Fe(III) ratio (denoted as (Fe(II)/Fe(III)) bound) in magnetite which was shown to vary with pH, as reported in Cheng et al.[56]. [Fe(II)]tot is the total concentration of Fe(II) in the suspension (solid + solution) and [Fe(II)]aq is the dissolved concentration of Fe(II), measured after filtration (0.2 µm, Whatman) of the magnetite suspension.

Results and discussion

Iron oxide NP physicochemical properties.

HR-TEM analyses provided images to assess the individual sizes and shapes of the nanoparticles (Fig. 1). Magnetite and maghemite oxides both displayed rounded shapes and similar sizes with average diameters of 7 ± 2 nm and 6 ± 2 nm (Table 1), suggesting that the oxidation of magnetite to maghemite did not impact the particle size. Accordingly, BET surface area for maghemite (131 m^2g^{-1}) is relatively close to that of magnetite (115 m^2g^{-1}) (Table 1). Hematite displayed different morphologies with rhombohedral shapes measuring 28 nm-wide and 39 nm-long on average, with a surface area of 49 m^2g^{-1} (Table 1). No significant changes were reported for neither HA- nor PC-coated magnetite from TEM images, suggesting that the coating process did not modify the morphology of magnetite. Although the surface area was not determined for coated materials, no significant modification is expected, according to previous findings[57].

ATR-FTIR spectroscopy

The IR spectrum recorded for of Fe_3O_4, HA-Fe_3O_4- and PC-Fe_3O_4 showed successful coating of HA and PC on magnetite surfaces (Fig. 2). In the spectra of HA-Fe_3O_4, the presence of an acid carboxylic group was proven by the vibrational bands at 1410 cm^{-1} and 1614 cm^{-1} [58-60]. In the spectra of PC-Fe_3O_4, the absorption bands at 1239 cm^{-1}, 1088 cm^{-1} and 970 cm^{-1} were assigned to the presence of the PO_4^{3-} group, suggesting that PC was coated on the magnetite surface[61, 62].

Oxidation kinetics

The variation of total Fe(II)/Fe(III) ratio versus time for magnetite suspension exposed to air is characterized by a two-steps' behavior. Over the four first days (0-96 h), a sharp decrease in total

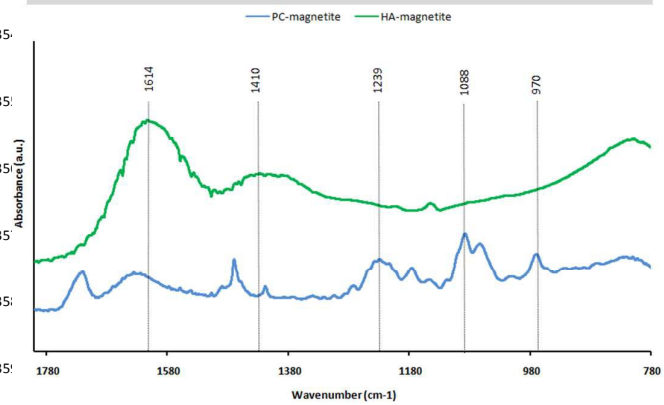

Fig 2: ATR-FTIR spectra of HA-magnetite and PC-magnetite in the range 780-1800 cm^{-1} obtained from 0.5 g L^{-1} NP suspensions at pH= 6.

View Article Online
DOI: 10.1039/C7EN01159H

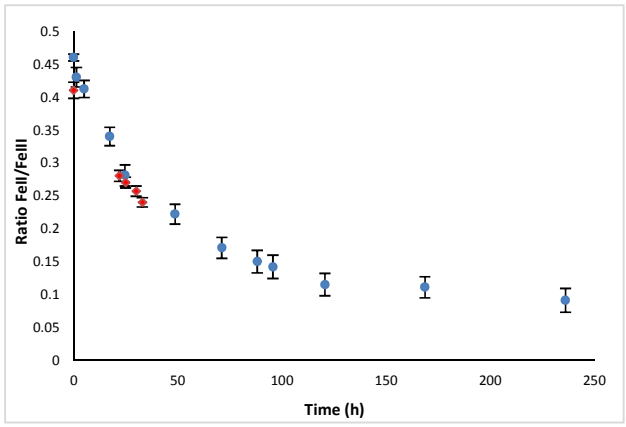

Fig 3: Evolution of the total Fe(II)/Fe(III) ratio (blue circles) and bound Fe(II)/Fe(III) ratio (red diamond) as a function of time. The reaction was performed with 2.5 g L^{-1} magnetite NP at pH = 7.5 in oxic conditions.

Fe(II)/Fe(III) ratio was observed (from 0.46 to 0.09). During this first stage, the bound Fe(II)/Fe(III) ratio was also decreased for magnetite as represented by red symbols in Figure 3. Then, the total Fe(II)/Fe(III) ratio slightly decreased beyond 5 days to reach 0.09 at the end of the experiment (236 h). As expected from the magnetite solubility at pH = 7.5[1], very little difference was observed between the total and bound Fe(II)/Fe(III) ratios.

Aggregation state

To assess the effect of pH and the effects of coating, laser diffraction analyses were performed on each iron oxide (Fe_3O_4, HA-Fe_3O_4, PC- Fe_3O_4, γ-Fe_2O_3 and α-Fe_2O_3) at five different pH values. For all experiments, the aggregation state was associated with the size distribution of the NP, which was described by considering the evolution of the sizes (based on number analyses) with the pH, occurrence rate and the polydispersity of the sizes (PDI, size range, mode and mean) of each iron oxide NP.

Effects of pH. The impact of pH on particle size distribution provides valuable information that could be used to distinguish the colloidal stability from the aggregation state of the various NP (Table 2). The different pH-dependent configurations highlighted the role of pHzpc in controlling NP aggregation through electrostatic interactions (Fig. 4). The effect of pH was studied by considering the evolution of the size distributions into four size classes (Fig. 4). The fractions were defined with regards to the most common sizes (representability) and depending on the way they vary with pH. However, it should be noted that fractions are not fully comparable to one another, as they were not spread out equally (i.e. fraction >0.4 µm (µm-scaled size class) as compared to 40-100 nm fraction (nm-scaled sizes)). The full-size distribution diagrams obtained from laser particle analyses as well as the precise occurrence rates (detectors) are provided in the Electronic Supporting Information (ESI).

It is worth noting that the total dissolved iron content was only detected in the magnetite suspension at pH = 3 and pH = 4 (90 and 23 µmol L^{-1} respectively). These values correspond to 1.4 % and 0.4 %, respectively, of the total iron amount in NP suspension. For HA- and PC-magnetite samples, no dissolved iron was detected regardless of the investigated pH.

Magnetite. The NP size distribution displayed two configurations: at pH = 5, 4 and 3, magnetite NP showed colloidal stability as compared to their size distribution at pH = 6 and 7.5. Magnetite size distribution at acidic pH was characterized by a high proportion of small NP (≤0.04 µm), and the occurrence of few dispersed µm-scaled aggregates (with sizes ranging between 1.6 µm and 32 µm). Such distribution allowed a large amount of NP not to sediment, as defined by Buffle et al.[63]. When the pH increased to 6 and 7.5, the number of coarser 100-400 nm and 40-100 nm-sized aggregates increased as the proportion of small aggregates decreased. This is consistent with the measured pHzpc = 5.8 (in accordance with previously published values[4]), since aggregation is commonly favoured at pH close to the pHzpc. Therefore, particles exhibiting negative charges likely formed coarser aggregates when the pH approached the pHzpc because of favorable electrostatic interactions[64].

	Magnetite		HA-Magnetite		PC-Magnetite			Maghemite			Hematite	
pH	6	5	4	3	7.5	5	4	7.5	6	5	7.5	5
Range (µm)	0.04 - 0.4; 1.6 - 32	0.04 - 0.4; 1.6 - 32	0.04 - 18	0.04 - 0.4; 1.1 - 19	0.04 - 0.4; 1.2 - 45	0.04 - 0.4; 1.1 - 40	0.04 - 0.4; 1.6 - 56	0.04 - 0.4; 1.6 - 28	0.04 - 0.4; 1.6 - 28	0.5 - 0.7; 1.1 - 28	0.04 - 6	0.04 - 0.4; 1.1 - 12
Mode (µm)	0.04	0.04	0.04	0.04	0.04	0.04	0.04	0.04	0.04	8	1.4	0.04
Mean (µm)	1.3	0.9	0.4	0.6	1.1	0.8	1.3	4.1	1.1	6.8	1.3	0.5
Median (µm)	0.07	0.04	0.04	0.07	0.07	0.04	0.07	0.2	0.04	7	1.2	0.04
PDI	1.38	2.74	13	5	1.9	3.4	1.3	0.56	2.06	0.72	4.8	7.6

Table 2: Size distribution characteristics of each NP at some typical pH (aggregation state versus colloidal stability). The table shows the size-range, mode, mean size, median value and the PDI (polydispersity index) of magnetite, HA-coated magnetite, PC-coated magnetite, maghemite and hematite. High PDI have values up to 1.0 and very high PDI are up to 2.0.

View Article Online
DOI: 10.1039/C7EN01159H

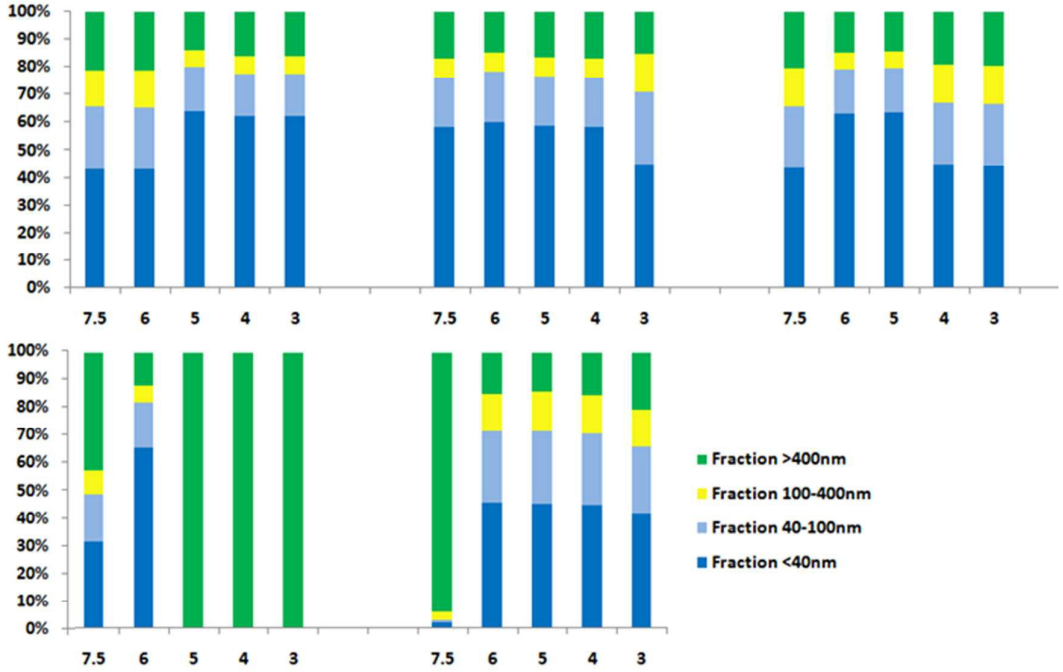

Fig 4: Evolution of four typical size-class (proportion in %) with pH for a) magnetite, b) HA-magnetite, c) PC-magnetite, d) maghemite and e) hematite. Below the histograms, the table displayed the percentages of each fraction for typical pH (3, 4, 5, 6 and 7.5).

HA-Magnetite. HA-magnetite nanoparticles displayed both a continuous size distribution (pH = 4 to pH = 7.5) and a dual size distribution (pH = 3). In both cases, fraction below 0.04 µm was more important but their proportion decreased as the pH decreased from pH = 4 to 3. This decrease was accompanied by a slight increase in 40–100 nm-sized fraction and an increase in the proportion of coarser intermediate 100-400 nm NP size-class, which appeared to be more dependent upon pH than other fractions. The occurrence rate of the coarse aggregate fraction (>0.4 µm and >1.1 µm) remained constant regardless of the pH, hence a lower pH implied a moderated aggregation with small (≤0.04 µm) particles aggregating in only slightly coarser (0.05-0.4 µm) aggregates. Thus in HA-coated iron oxide NP, HA appeared to be an effective organic stabilizer towards iron oxide NP as previously demonstrated[65, 66].

PC-Magnetite. PC-magnetite nanoparticles highlighted two size distribution depending on the pH. At pH = 6 and 5, the size distribution was similar to that of bare magnetite at acidic pH (pH = 3 and pH = 4) where the colloidal stability displayed its maximum. At pH = 7.5, 4 and 3, Fe_3O_4-PC showed a similar size distribution to bare magnetite at pH >6, when it aggregated. When the pH decreased to pH = 4 and pH = 3, small aggregates (≤ 0.04 µm) were still the most common but in a lower proportion which was compensated by a higher amount of the three other coarser size fractions (in order: 40-100 nm; >1.6 µm and 100-400 nm). Although 100-400nm-sized aggregates were still the least common, this fraction was the most sensitive to pH as its proportion more than doubled from pH 6 and 5 to pH 4 and 3.

Maghemite. The size distribution displayed three configurations as distinct fractions whose proportions were strongly controlled by the pH. At a weak basic pH (pH = 7.5), the distribution was highly polydispersed and made up of coarse aggregates (>0.4 µm), which spread over a large size range. Maghemite NP displayed colloidal stability at pH = 6 with a size distribution similar to that of magnetite. However, when the pH decreased to a more acidic pH (pH = 5, 4 and 3), small-sized NP and NP aggregates disappeared to form much coarser aggregates with almost exclusively µm-scale sizes (>1 µm). Thus, the maghemite size distribution would be in good agreement with a high pHzpc close to 7.5[67, 68], as it became coarser than at pH = 6, but the high aggregation observed from pH = 3 to 5 suggested the possible implication of parameters other than electrostatic interactions to drive maghemite colloidal stability.

Hematite. The hematite size distribution showed two pH-dependent size distribution patterns. At pH = 7.5, the sizes were continuously distributed with a unique narrow size range composed of coarse homogeneous sizes displaying high polydispersity (multimodal distribution centered on 1.4 µm). When the pH decreased to pH = 6 and lower, the pH drastically modified the hematite size distribution to a more stable aggregation state[69] characterized by a monomodal distribution (0.04 µm) and higher abundance of finer particles (<0.4 µm). In accordance with the hematite pHzpc at pH = 8.2, hematite NP tended to aggregate when the pH reached pH = 7.5.

Effects of coating. The physico-chemical characteristics obtained from the combination of HR-TEM and ATR-FTIR showed

View Article Online
DOI: 10.1039/C7EN01159H

that HA have been successfully coated onto magnetite NP. According to HR-TEM images, HA coating on magnetite did not affect the original morphology and size of the precursor NP. As the surface modification with HA provided primarily acidic functional groups, the HA-coated magnetite pHzpc likely decreased to a lower pH (pHzpc = 2.3). Accordingly, magnetite-HA promoted colloidal stability from pH = 7.5 to pH = 4 because of repulsive electrostatic interactions. The aggregation observed at pH = 3 - close to the new pHzpc - would then be explained by the lack of negative surface sites to compensate for the protonation induced by the H^+ concentration increase in the aqueous solution. Both HA and bare magnetite evidenced that the proportion of their size- fractions was strongly controlled by the pH, which induced either colloidal stability or aggregation. Nevertheless, HA coating promoted smaller-sized aggregates as well as a narrower size distribution and more homogeneous stable sizes (especially for coarser particles (>0.4 µm)) compared to bare magnetite (Table 2). This enhanced stabilization may stem from a HA steric barrier that helped maintain a space between the particles to prevent the aggregation of NP[70, 71]. Similar to the HA coating, the PC surface modification did not affect the size and morphology of magnetite. Magnetite coated with PC displayed a different colloidal behaviour as compared to bare magnetite. As PC imparted both negative and positive surface groups on the surfaces of the NP (glycerophosphate group, trimethylethanolammonium group), and because of the complex and heterogeneous surface structures that are generated by adsorbed PC[72], PC-coated nanoparticles likely displayed variable colloidal behaviours. As compared to magnetite, PC-NP showed similar size proportions and repartition although the magnetite-PC coarse fraction displayed a few large aggregates (hence its wider size range, see Table 2) regardless of the pH. PC-NP were thus probably able to form highly contrasted structures (according to their size) suggesting that PC-coated magnetite did not entirely depend on electrostatic interactions but also on steric forces[72].

Effects of iron oxide intrinsic physicochemical properties. The oxidation of magnetite (Fe_3O_4) to maghemite (γ-Fe_2O_3) did not change morphology and particle size. Maghemite still displayed a higher surface area (131 $m^2\ g^{-1}$) than magnetite (115 $m^2\ g^{-1}$) and oxidized NP very likely yielded intrinsic compositional differences. These modifications probably resulted in a higher surface potential thereby explaining the variable size distributions observed as the pH changed. Maghemite NP aggregation was favoured at acidic pH (equal or below 5), which would be in good agreement with their high surface potential. Indeed, the tendency to form large aggregates at these pH values likely resulted from a high energetic barrier that had to be overcome at the mineral surfaces[73]. Indeed, increasing NP surface to volume ratio leads to a higher surface energy which induces aggregation between particles. As hematite displayed a much lower surface area, the higher colloidal stability observed over a wide pH range may result from a lower energetic barrier at the surface of the particles in accordance with NP having a relatively lower surface potential. Hematite stability would thus be related, in part, to its smaller surface area and surface potential. However, the typical aggregation behaviour of hematite NP

Environmental perspectives. Aggregation and stabilization have significant effects on the mobility, reactivity and environmental fate of NP. Once released in surface waters, unstable particles tend to agglomerate, sediment or flocculate or they preferentially adsorb onto bigger particles or surfaces[77]. As a result, aggregated NP that form larger colloids with a possible smaller surface area are less easy to transport and do not get through the soil as easily as smaller particles[78]. As aggregated NP become less mobile, they may become more ineffective in acting as nutrient carriers[79]. It is also more difficult for these colloids to be taken up by plants and living organisms as they are less soluble than their smaller counterparts[80]. The dissolution of NP induces the mobilization of ions which are likely complexed with molecules that foster their absorption by plants and animals. In addition, depending on their concentration and speciation as well as on the physiology of the organism that absorbs it, metal atoms or ions can be either positive nutrients or toxic elements. On the other hand, aggregation may directly affect NP toxicity towards living organisms since smaller NP have been shown to penetrate the cell walls of certain species more easily[81, 82]. Considering the pH effect, the physicochemical properties of the soil solution have to be considered in order to accurately assess the fate of NP in the environment. NP intrinsic properties, such as their surface chemistry, are also of prime importance since they are involved in both electrostatic and steric interactions, which may impact their dispersion, bioavailability and biocompatibility[83].In natural waters and surficial aerobic environments, NP likely undergo many surficial modifications and become embedded in matrixes or functionalized with specific molecules[84]. As a result, these attached molecules can both passivate and/or confer their own properties to mineral surfaces; e.g. polyanionic HA coating on magnetite, resulting in a lower pHzpc and enhanced colloidal stability. In addition, HA coating - as well as PC covering - might passivate iron oxide NP surfaces to yield a steric barrier that prevents Fe leakage from mineral surfaces and the ageing of the magnetic core by oxidation. HA, which are ubiquitous in most aquatic systems, display a specific affinity for iron oxide NP as well as trace elements and therefore HA-iron oxide NP complexed structures may also enhance ETM adsorption to NP. However, although natural coatings demonstrated improved iron oxide NP stability and reactivity, their effects depend upon the amount and chemical composition of the substances[4].

The rapid oxidation of magnetite into maghemite is important since iron plays an active redox catalytic role in many energy transfer and electron transfer processes[85-87]. The iron oxide redox state also plays a key role in specific anaerobic environments where Fe(II) and Fe(III) are used as energetic catalysts for bacteria[88, 89]. Finally, the transformation of magnetite into maghemite is also relevant considering its adsorption capacity towards environmental compounds[90]. Several questions are raised from these environmental considerations, especially, what are the impacts of these modifications regarding iron oxide NP reactivity?

DOI: 10.1039/C7EN01159H

Conclusions

The pH appears to be a key driver in controlling iron oxide NP colloidal behaviour as resulting from protonation and deprotonation reactions of surface hydroxyl-groups. Surface modifications also implied considerable effects on iron oxide NP colloidal stability as they promoted electrostatic interactions. In contrast to PC, HA was shown to be particularly efficient in enhancing magnetite colloidal stability. Magnetite seems to be highly unstable in aerobic conditions. The oxidation of magnetite into maghemite modified its surface chemistry and surface area, and these modifications resulted in higher aggregation at most pH values. Compared to maghemite, hematite appeared to be less sensitive to pH and displayed a lower surface area and surface potential. Both hematite and maghemite displayed high aggregation size distributions at different pH values.

Considering the widespread use of iron oxide NP and their subsequent release in the environment, their fate and behaviour in soils and natural waters raise many environmental questions not only in terms of their possible impacts on living organisms but also for their mobility and fate in ecosystems. Therefore, more attention should be paid for the understanding of colloidal and chemical stabilities of iron oxide NP as it is likely involved in many major interactions within the environment.

Acknowledgements

We are thankful to François Pustoc'h for the time as well as the thorough advices he gave us to conduct laser particle analyses at the CReAAH (University of Rennes1). Dr Patricia Benard-Rocherullé and Dr Vincent Dorcet (ISCR, University of Rennes1) are deeply acknowledged for DRX and MET studies, respectively. Dr Fabienne Gauffre is thanked for her kind help to perform NTA measurements. Last, Dr S. Mullin is acknowledged for post-editing the English style (http://www.proz.com/profile/677614). This study was funded by both the CNRS-INSU/INEE EC2CO and the Interdisciplinarity Mission programs through 'NanoOrgaTraces' and 'ALIEN' projects, respectively both awarded to Mathieu Pédrot and the University Rennes 1 through 'Défis Scientifiques Emergents' program awarded to Aline Dia.

References

1 R. M. Cornell and U. Schwertmann, 2nd edition, *http://trove.nla.gov.au/version/36973177*, 2003, Edited by Wiley-VCH, 664p.

2 M. F. Hochella Jr, S. K. Lower, P. A. Maurice, R. L. Penn, N. Sahai, D. L. Sparks and B. S. Twining, *Science*, 2008, **139,** 1631.

3 A. Afkhami, M. Saber-Tehrani and H. Bagheri, *Desalination*, 2010, **263**, 240.

4 M. A. Ahmed, S. M. Ali, S. I. El-Dek and A. Galal, *Materials Science and Engineering B,* 2013,**178**, 744.

5 A. K. Gupta and M. Gupta, *Biomaterials,* 2005,**26**, 3995.

6 S. Laurent, J.-L.Bridot, L. Van der Elst and R. N. Muller, *Future Medicinal Chemistry,* 2010, **2(3)**, 427.

7 H. Guo and A. Barnard, *Journal of Materials Chemistry A*, 2013, **1**, 27.

8 M. Schindler and M. F. Hochella Jr., *Geology*, 2016, **44**, 515.

9 S. C. Löhr, D. T. Murphy, L. D. Nothdurft, R. Bohlar, S. Piazolo and C. Siegel, *Geochimica and Cosmochimica Acta*, 2017, **200**, 25.

10 C. W. Isaacson, M. Kleber and J. A. Field, *Environmental Science & Technology*, 2009, **43**,6463.

11 B. Nowack and T.D. Bucheli, *Environmental Pollution*, 2007, **150**, 5.

12 M. Auffan, J. Rose, J.-Y.Bottero, G. V. Lowry, J.-P.Jolivet and M.-R.Wiesner, *Nature Nanotechnology*, 2009, **4**, 634.

13 G. V. Lowry, K. B. Gregory, S. C. Apte and J. R. Lead, *Environmental Science & Technology*, 2012, **46**, 6893.

14 S. C. N. Tang, I. and M. C. Lo, *Water Research*, 2013, **47**, 2613.

15 M. Vitkova, S. Rakosova, Z. Michalkova, M. Komarek, *Journal of Environmental Management*, 2017, **186**, 268.

16 P. N. Dave and L. V. Chopda, *Journal of Nanotechnology*, 2014, **2014**, 1.

17 A. Aftabtalab, H. Sadabadi, CH. Shilpa Chakra, K. V. Rao, S. Shaker and E. Privilege Mahofa, *International Journal of Scientific & Engineering Research*, 2014, **5(1)**,1419.

18 S. R. Chowdhury and E. K. Yanful, *Journal of Environmental Management*, 2013, **129**, 642.

19 L. R. Khot, S. Sankaran, J. M. Maja, R. Ehsani and E. W. Schuster, *Crop Protection*, 2012, **35**, 64.

20 E. Navarro, A. Baun, R. Behra, N. B. Hartmann, J. Filser, A-J.Miao, A. Quigg, P. H. Santschi and L. Sigg, *Ecotoxicology*, 2008,**17**, 372.

21 A. Valdiglesias, N. Fernandez-Bertolez, G. Kiliç, C. Costa, S. Costa, S. Fraga, M. J. Bessa, E. Pasaro, J. P. Texeira and B. Laffon, *Journal of Trace Elements in Medicine and Biology*, 2016, **38**, 53.

22 R. Podila and J. M. Brown, *Journal of Biochemical and Molecular Toxicology*, 2013, **27(1)**, 50.

23 W. Wu, Z. Wu, T. Yu, C. Jiang and Woo-Sik Kim, *Sci. Technol. Adv. Mater*., 2015, **16**, 023501.

24 O. Veiseh, J. W. Gunn, M. Zhang, Advanced Drug Delivery Review, 2010, **62**, 304.

25 Y. Ju-Nam and J. R. Lead, *Science of the Total Environment*, 2008, **400**, 414.

26 A-H. Lu, E.L. Salabas and F. Schüt, Angew. Chem. Int. Ed., 2007, **46**, 1244.

27 D. Maity and D.C. Agrawal, *Journal of Magnetism and Magnetic Materials*, 2007, **308**, 46.

28 M. M. Can, M. Coskun and T. Firat, *Journal of Alloys and Compounds*, 2012, **542**, 241.

29 A. Lassoued, M. S. Lassoued, B. Dkhil, A. Gadri and S. Ammar, *Journal of Molecular Structure*, 2017, **1141**, 99

30 S. C. Pang, S. F. Chin and M. A. Anderson, *Journal of Colloid and Interface Science*, 2007, **311**, 94.

View Article Online
DOI: 10.1039/C7EN01159H

31 L. Peng, P. Qin, M. Lei, Q. Zeng, H. Song, J. Yang, J. Shao, B. L. and J. Gu, *Journal of Hazardous Materials*, 2012,**209-210**,193.

32 E. Tombacz, Z. Libor, E. Illès, A. Majzik and E. Klumpp, *Organic Geochemistry*, 2004, **35,** 257.

33 A. M. Vindedahl, J. H. Strehlau, W. A. Arnold and R. L. Penn, *Environmental Science: Nano, Critical Review*, 2016, **3**, 1.

34 M. Baalousha, *The Science of the Total Environment*, 2009, **407**, 2093.

35 E. Illes and E. Tombacz, *Journal of Colloid and Interface Science,* 2006, **295**,115.

36 E. Tombacz, I.Y. Toth, D. Nesztor, E. Illés, A. Hadju, M. Szekeres and L. Vékas, *Colloids and Surfaces A: Physicochemical and Engineering Aspects*, 2013,**435**, 91.

37 A. Hajdú, E. Illés, E. Tombácz and I. Borbáth, *Colloids and surfaces A: Physicochemical and Engineering Aspects*, 2009, **347**, 104.

38 J. Hao, C. Cleveland, E. Lim, D. R. Strongin and M. A. A. Schoonen, *Geochemical Transactions*, 2006, **7:8**, 1.

39 X. V. Zhang, T. A. Kendall, J. Hao, D. R. Strongin, M. A. A. Schoonen and S. T. Martin, *Environmental Science & Technology*, 2006, **40**, 1511.

40 J. Giri, S. G. Thakurta, J. Bellare, A. K. Nigam and D. Bahadur, *Journal of Magnetism and Magnetic Materials*, 2005, **293**, 62.

41 S. Chatterjee, M. Krikorian, H. D. Gafney and B. Gersten, *Material Research Society*, 2011, **1061**, MM09-08.

42 R. Frison, G. Cernuto, A. Cervellino, O. Zaaharko, G. M. Colonna, A. Guagliardi and N. Masciocchi, *Chemistry of Materials*, 2013, **25**, 4820.

43 U. S. Khan, Amanullah, A. Manan, N. Khan, A. Mahmood and A. Rahim, *Material Science-Poland*, 2015, **33(2)**, 278.

44 I. Nedkov, T. Merodiiska, L. Slavov, R.E. Vandenberghe, Y. Kusano and J. Takada, *Journal of Magnetic Materials*, 2006, **300**, 358.

45 H. Shokrollahi, *Journal of Magnetism and Magnetic Materials*, 2017, **426**, 74.

46 L. Charlet G. Morin, J. Rose, Y. Wang, M. Auffan, A. Burnol and A. Fernandez-Martinez, *ComptesRendus Geoscience*, 2011, **343**, 123.

47 L. Chekli, S. Phuntsho, M. Roy, E. Lombi. E. Donner and H. K. Shon, *Water Research*, 2013, **47**, 4585.

48 W. Li, J. Wu, C. Kim and J. D. Fortner, *Environmental Science &Technology*, 2014, **48(20)**, 11892.

49 A. Navrotsky, L. Mazeina and J. Majzlan, *Science*, 2008, **319**, 1635.

50 R. Massart, *IEEE Transactions on Magnetics*, 1981, **17**,1247.

51 S. E. Khalafalla and G. W. Reimers, *IEEE Transactions on Magnetics*, 1980, **16(2)**, 178.

52 Z. B. Anna, B. Patricyja, J. Petr, E. Petrovsky, B. Pavel, H. Daniel, *Colloids and Surfaces B: Biointerfaces,* 2016, **141**, 389.

53 D. Yeghicheyan, C. Bossy, M. Bouhnik Le Coz, C. Douchet, G. Granier, A. Heimburger, F. Lacan, A. Lanzanova, T. C. C. Rousseau, J.L. Seidel, M. Tharaud, F. Candaudap, J. Chmeleff, C. Cloquet, S. Delpoux, M. Labatut, R. Losno, C. Pradoux Y. Sivry and J. E. Sonke, *Geostandards and Geoanalytical Research*, 2013, **37(4)**, 449.

54 C. A. Gorski and M. M. Sherer, *American Mineralogist*, 2010, **95**, 1017.

55 P. Komadel and J. W. Stucki, *Clays and Clay Minerals*, 1988, **36(4)**, 379.

56 W. Cheng, R. Marsac and K. Hanna, *Environ. Sci. Technol*., 2018, **52 (2)**, 473.

57 J. Lohdia, G. Mandarano, N. J. Ferris, P. Eu and S. F. Cowell, *Biomedical Imaging and Intervention Journal*, 2010**,6(2)**, 1.

58 H. Niu, D. Zhang, S. Zhang, X. Zhang, Z. Meng and Y. Cai, *Journal of Hazardous Materials*, 2011, **190**, 559.

59 J.-F. Liu, Z.-S. Zhao and G.-B.Jiang, *Environmental Science & Technology*, 2008, **42**, 6949.

60 S. Koesnarpadi, S. J. Santosa, D. Siswanta and B. Rusdiarso, *Procedia Environmental Sciences* 30 (2015, 103.

61 S. Debnath, D. B. Hausner, D. R. Strongin and J. Kubicki, *Journal of Colloids and Interface Sciences*, 2010, **341**, 215.

62 Q.-C. Le, M.-H. Ropers, H. Terrisse and B. Humbert, *Colloids and Surfaces B: Biointerfaces*, 2014, **123**, 150.

63 J. Buffle, K. Wilkinson, S. Stoll, F. Montserrat, Z. Jingwu, *Environmental Science & Technology*, 1998, **32(19)**, 2899.

64 A. Kraynov and T. E. Müller, In *Applications of Ionic Liquids in Science and Technology*, 2011, Edited by Prof. S. Handy (516 pages), 235.

65 M. Pédrot, A.L. Boudec, M. Davranche, A. Dia, O. Henin, *Journal of Colloid and Interface Science*, 2011, **359**, 75.

66 D. Palomino and S. Stoll, *Journal of Nanoparticle Research*, 2013, **15(2)**, 1428.

67 N. Fauconnier, J. N. Pons, J. Roger and A. Bee, *Journal of Colloid and Interface Science*, 1997,**194**, 427.

68 L. Vayssieres, *J. Phys. Chem. C,* 2009, **113**, 4736.

69 K. Shimizu, S. V. Sokolov and R. G. Compton, *Colloid and Interface Science Communications*, 2016, **13**, 19.

70 S. Ghosh, W. Jiang, J. D. McClements and B. Xing, *Langmuir*, 2011*,* **27**, 8036.

71 S. F. Meideros, J. O.C. Filizzola, V. F.M. Fonseca, P. F.M. Oliveira, T. M. Silva, A. Elaissari and A. M. Santos, *Materials Letters*, 2015, **160**, 522.

72 R. Michel and M. Gradzielski, *International Journal of Molecular Science*s, 2012, **13**, 11610.

73 K. A. D. Guzman, M. P. Finnegan and J. F. Banfield, *Environmental Science & Technology*, 2006, **40**, 7688.

74 M. D. Carvalho, F. Henriques, L. P. Ferreira, M. Godinho and M. M. Cruz, *Journal of Solid State Chemistry*, 2013,**201**, 144.

75 E. Alp and N. Aydogan, *Colloids and Surfaces A: Physicochemical and Engineering Aspects*, 2016, **510**, 205.

76 D. Dickson, G. Liu, C. Li, G. Tachiev and Y. Kai, *The Science of the Total Environment*, 2012, **429**, 170.

77 A. M. Badawy, A. A. Hassan, K. G. Scheckel, M. T. Suidan and T. M. Tolymat, *Environmental Science and Technology*, 2013, **47**, 4039.

78 M. Komarek, A. Vanek and V. Ettler, *Environmental Pollution*, 2013, **172**, 9.

View Article Online
DOI: 10.1039/C7EN01159H

79 C. Claudio, E. di Iorio, Q. Liu, Z. Jiang, V. Barron, *Journal of Nanoscience and Nanotechnology*, 2017, **17(7)**, 4449.
80 I. A. Mudunkotuwa and V. H. Grassian, *Journal of Environmental Monitoring*, 2011, **13(5)**, 1135.
81 J. Bauman, J. Köser, D. Arndt and J. Filser, *The Science of the Total Environment*, 2014, **484**, 176.
82 K. Powers, M. Palazuelos, B. M. Moudgil and S. M. Roberts, *Nanotoxicology*, *2007,***1 (1)**, 42.
83 R. K. Das, S. K. Brar and M. Verma, *Trends in Biotechnology*, 2016, **34(6)**, 440.
84 D. Lin, S. D. Story, S. L. Walker, Q. Huang, W. Liang and P. Cai, *Environmental Pollution*, 2017, **228**, 35.
85 K. S. Siddiqi, A. ur Rahman, Tajuddin and A. Husen, *Nanoscale Research Letters*, 2016, **11**, 498.
86 H. Wu, J. J. Yin, W. G. Wamer, M. Zeng and Y. M. Lo, *Journal of Food and Drugs Analysis*, 2014, **22**, 86.
87 S. K. Chaudhuri, J. G. Lack, J. D. Coates, *Applied and Environmental Microbiology*, 2001, **67**, 2844.
88 M. Posfai, T. Kasama, E. T. Simpson, R. K. K. Chong and R. E. Dunin-Borkowski, *ActaCrystallica*, 2006**, 62**, 39.
89 J.-Y. Bottero, M. Auffan, J. Rose, C. Mouneyrac, C. Botta, J. Labille, A. Masion, A. Thill and C. Chaneac, *ComptesRendus Geoscience*, 2011, **343**, 168.
90 M. Davranche, A. Dia, M. Fakih, B. Nowack, G. Gruau, G. Ona-Nguema, P. Petitjean, S. Martin and R. Hochreutener, *Chemical Geology*, 2013,**335**, 24.